Optics and Lasers in Engineering 160 (2023) 107242

Contents lists available at ScienceDirect

Optics and Lasers in Engineering

journal homepage: www.elsevier.com/locate/optlaseng

# A bilayer color digital image correlation method for the measurement of the topography of a liquid interface

Yao Huang [a,1], Xianfu Huang [b,c,1,*], Menglin Zhong [a], Zhanwei Liu [a,*]

[a] School of Aerospace Engineering, Beijing Institute of Technology, Beijing, 100081, PR. China
[b] State Key Laboratory of Nonlinear Mechanics (LNM), Institute of Mechanics, Chinese Academy of Sciences, Beijing, 100190, PR. China
[c] School of Engineering Science, University of Chinese Academy of Sciences, Beijing, 100049, PR. China

ARTICLE INFO

*Keywords:*
Topography measurement
Color speckle pattern
Digital image correlation
Virtual image
Virtual displacement field
Snell's law

ABSTRACT

One of the most essential characteristics of the liquid interface is the topography dominated by hydrodynamics or capillary effects. Although there have developed 3D imaging techniques for the measurement of such topography, their setups, operations and reconstructions are relatively complex and suffer from low efficiency. Here we report a bilayer color digital image correlation (BC-DIC) method for the measurement of the topography of a liquid interface. The basic principle of the new method is the refraction of beneath bilayer color speckle patterns at the liquid interface, which makes it possible to perform 3D reconstruction through 2D measurement of the virtual displacement field of the speckle patterns. The equations for BC-DIC in different situations are deduced and discussed in detailed. Validation experiments are carried out to reconstruct the topography of triangular prism, planoconvex, complex transparent surface and sloshing water surface. The results show that BC-DIC is feasible and accurate for measuring the topography of transparent objects, including liquid interface. This new method paves the way for investigating surface and interface phenomena, such as capillarity and wetting issues, hydrodynamics on liquid interface, etc.

## 1. Introduction

The measurement of liquid interfaces topography is of great significance in the research of surface and interfacial phenomena, such as liquid sloshing dynamics [1–4], hydrodynamics of water-walking insects [5–9], and capillarity and wetting issues [10–15], etc. For transparent liquids, it is generally difficult to measure their topographies due to strong transmittance, easy rheology and high reflection at interfaces [16]. Most of the traditional optical methods based on surface diffuse reflection are not applicable.

Currently, there are mainly two types of methods for measuring the topography of transparent liquids, namely, the specular reflection methods and the transmission methods. The first type is based on the specular reflection at the liquid interface, and typically represented by the fringe reflectometry [17, 18]. This kind of methods were first used for the measurement of solid objects with mirror surfaces, and has also been used to measure the deformation of liquid interfaces in recent years [18–20]. The specular reflection methods are very sensitive to the curvature of the measured interfaces. Therefore, when the slope of the liquid interfaces is too large, the reflected light may deviate from the camera's field of view, resulting in a dark field in the captured images, which cannot be used to measure the topography of liquid interfaces with large curvature. The second type of methods, i.e., the transmission methods, is mainly by placing a texture pattern on the bottom of the liquids, and setting a camera above the liquid interface to capture the texture images before and after the interface is deformed. The topography can be reconstructed through analyzing the distortion fields of the captured images. In this regard, many works have carried out [21–27]. For example, under the assumption of small deformation and paraxial, Mosiy et al. proposed free-surface synthetic Schlieren (FS-SS) method based on digital image correlation (DIC) [27]. They have really carried out a series pioneering studies in developing FS-SS for the measurement of free-surface of the topography of liquid surfaces [27–29]. Despite the elegant idea of the FS-SS, it suffers some drawbacks. In addition to meeting the assumption of single refraction and near optical axis, the FS-SS method is only suitable for liquid interface measurement with small deformation (the maximum deformation is no more than 2% of the liquid depth) because of is approximation of small angles at the refraction angle and incident angle of the optical path [27]. This is not applicable to the objects with large slope of interface. Earlier work of this kind of technique may traced back to Fouras et al. [26, 30]. Liu et al. [21, 31] obtained the initial value of the differential equation of the liquid interface height

* Corresponding authors.
*E-mail addresses:* huangxf@imech.ac.cn (X. Huang), liuzw@bit.edu.cn (Z. Liu).
[1] Yao Huang and Xianfu Huang are co-first authors.

https://doi.org/10.1016/j.optlaseng.2022.107242
Received 4 December 2021; Received in revised form 5 May 2022; Accepted 29 August 2022
Available online 9 September 2022

by increasing the initial depth of the liquid. The reconstruction speed of this kind of methods is slow, because it requires a tedious mathematical retrieval process.

Kolaas et al. [32] proposed bichromatic synthetic schlieren (BiCSS) for surface measurements, which mainly uses the refractive index difference between blue and near-infrared light to further improve the slope measurement range of the FS-SS method. The principle is the same as that of FS-SS [27], which adopts the paraxial hypothesis of light path with small liquid interface deformation. The difference is that BiCSS method uses two CCD cameras to separate the two colors of light. The topography of the liquid interfaces needs further calculation, because the direct solution is the slope of the liquid surface [32]. Moreover, their studies mainly focused on obtaining virtual image displacement difference of different colors on the same plane. Stereo method need at least two cameras to implement the measurement of topography [33–36]. When the deformation of liquid interface is fast, the correspondence and simultaneous triggering of multi-camera image acquisition is a problem. Moreover, in order to enhance the reflection effect, the reflection method usually needs to use some additive to enhance the liquid interface reflection.

In this paper, we propose a bilayer color DIC (BC-DIC) method for measuring the topography of liquid interfaces, which overcomes the shortcomings of the iterative process and the assumption of small deformation of liquid interfaces in the transmission methods. We shall present the principle of the method and derive the theoretical formulas in §2. The new method is validated and evaluated by a series of topography measurements of transparent objects, as well as applied to the dynamic deformation measurement of the liquid interface in §3 and §4. Finally, we give a brief conclusion of the BC-DIC method.

## 2. Methodology

### 2.1. Principle

A common scenario in life is when we observe the liquid in the container from the top—here we assume that there is a solid object in the liquid of at the bottom—if the liquid is shaking or tilting which causes the liquid interface to deviate from its original position, what we see the object (virtual image) will be correspondingly distorted with the topography of the liquid interface due to the refraction. It can also be observed directly that there is a positive correlation between the distortion of the observed object and the topography of the liquid interface. This is not difficult to understand: When the topography of the liquid interface fluctuates, it is similar to placing an array of convex or concave lenses above the object, which distorts the observed image of the object. If the above object is a two-dimensional speckle pattern and placed on the bottom of the liquid, the observed pattern from the top will be deformed according to the topography of the liquid interface. This is the basic principle of the Transmission-Speckle Correlation (TSC) method [6, 21] and Fringe Transmission Technique (FTT) [2, 22-25] proposed by Liu et al., and FS-SS method by Moisy et al. [27]. This type of methods needs to know at least one row of liquid height as the initial value of the iterative calculation (usually the edge of the field of view). Moreover, the iterative calculation involves complex and nonlinear computing. And errors will be accumulated and transferred to the subsequent calculations [23].

Can the above principle and calculations be further optimized, that is, the topography of the liquid interface can be easily reconstructed without iterative calculating and initial values? The answer is yes. In this paper, we report a BC-DIC method, which settles the shortcomings of the iteration and the assumption of small deformation, to greatly simplify the reconstruction of the liquid interface. The schematic diagram of the BC-DIC is shown in Fig. 1. First, two transparent films are printed with blue and red speckles respectively. And they are glued onto the upper-layer and bottom-layer of a transparent flat glass. Then the glass with bilayer color speckle patterns is placed under the liquid, as depicted in Fig. 1(a). When viewed from the top of the liquid interface, a coupled blue-red virtual image of the color speckle patterns can be seen. The reason why red and blue colors are selected is that their contrast is strong enough, so it is convenient to decouple the color patterns. As shown in Fig. 1(b), a cross section PP′ is taken to analyze the optical path used to measure the topography of the liquid interface. For a certain light emitted from point N on the liquid interface, it first passes through point D on the bottom surface of the glass and then point C on the upper surface. After being refracted multiple times on the glass surfaces at points B and A, it emerges from the upper liquid interface and is finally collected by a light receiver on the top of the interface (e.g., a CCD camera). From the perspective of the receiver, the virtual images of C and D are at the right above of their own positions if the liquid interface is horizontal. When the liquid interface is deformed and forms a changing topography, it can be seen that due to the rise and fall of the liquid interface, the virtual images of point C and D move to the line ND′ caused by refraction, resulting in virtual displacements $S_1$ and $S_2$ contained in the color speckle patterns. It is obvious that the distance from horizontal and the slope at point N are correlated with $S_1$ and $S_2$, indicating the topography may be measured by analyzing virtual displacements of color speckle patterns.

In order to reveal the relation between the topography $h$ of the liquid interface (i.e., the distance from the bottom to the upper interface of the liquid) and virtual displacements $S_1$, $S_2$, we first consider the relation between the incident and refraction angles given by the Snell's law:

$$n_1 \sin\gamma = n_2 \sin\beta_2 = n_2 \sin\alpha_2 = n_3 \sin\beta_3 \tag{1}$$

where $n_1$, $n_2$, $n_3$ are the refractive indexes of the liquid, glass and air, respectively. $\alpha_2$, $\beta_3$, $\beta_2$, $\gamma$ are incident angles of DC, CB, BA and AN.

Eq. (1) gives:

$$\begin{cases} \beta_3 = \arcsin\frac{n_3}{n_2}\sin\alpha_2 \\ \gamma = \arcsin\frac{n_1}{n_2}\sin\alpha_2 \end{cases} \tag{2}$$

As shown in Fig. 1(b), the right triangle gives:

$$\tan\alpha_2 = \frac{S_2 - S_1}{d_1} \tag{3}$$

where $d_1$ is the thickness of the flat glass with color speckle patterns ($d_1 = |C'D'|$).

Similarly, in the right triangle the height between the interface and the bottom of the liquid $h$ is expressed as:

$$h = \frac{L}{\tan\gamma} \tag{4}$$

where $L$ is the distance from the intersection of the incident point A to the vertical line of point N (i.e., $|AA'|$ in Fig. 1(b)), which is given by:

$$L = S_1 - d_2\tan\beta_2 - d_3\tan\beta_3 \tag{5}$$

where $d_2$ is the thickness of the bottom glass of the tank ($d_2 = |A'B'|$; $d_3$ is the distance between the color speckle glass and the bottom glass of the tank ($d_3 = |B'C'|$).

In the actual reconstruction of the topography of the liquid interface $h$, there are three measurement schemes according to the relative positions of the bottom of the liquid and the speckle patterned glass. Their equations for the reconstruction are slightly different and are respectively derived as follows.

(1) In the most general case, there is airgap between the upper-layer speckle pattern and the liquid tank. Equations (1∼5) lead to:

$$h = \frac{S_1 - d_3\tan\alpha_2 - d_2\tan\beta_3}{\tan\gamma} \tag{6}$$

As shown in Fig. 1(b), the greater the airgap distance, the greater the virtual image displacement $S_1$ and $S_2$ of the upper and bottom speckle patterns. It does not affect the size of each incident angle and refraction angle. However, when the air gap is too large, the excessive displacement will lead to the decorrelation of speckle, and even further make

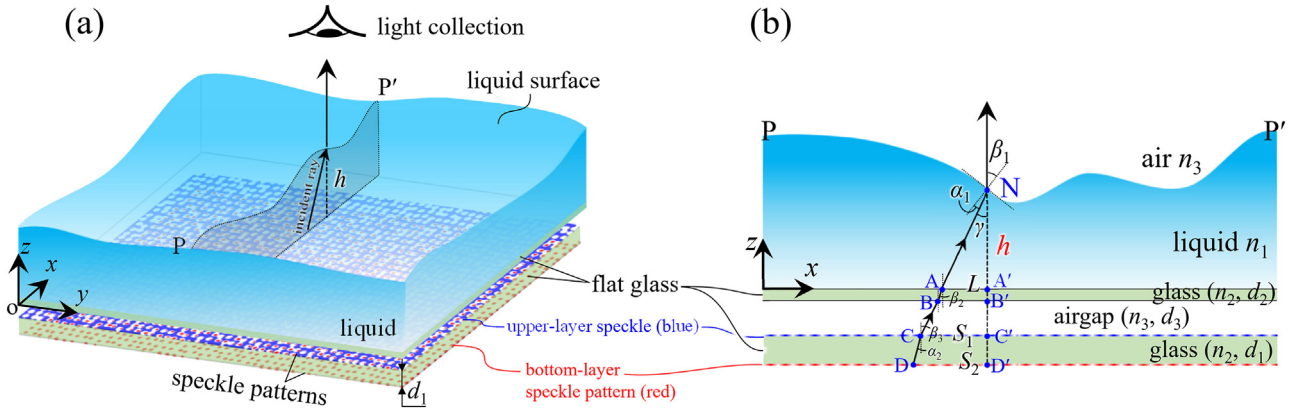


**Fig. 1.** A schematic diagram of the BC-DIC method. (a) Light path in a space coordinate system. The color speckle patterns are tightly attached to flat glass located under the liquid, and an airgap with a depth of $d_3$ may exist between the liquid and upper-layer spackle pattern; (b) An arbitrary cross section PP′ in (a). Nomenclature: Point B and A are located on the surfaces of the upper flat glass. The angles that DC, CB, BA and AN form with the vertical line are $\alpha_2$, $\beta_3$, $\beta_2$ and $\gamma$, respectively (marked in (b)). $\beta_1 = \alpha_1 + \gamma$; $|C'D'| = d_1$, $|A'B'| = d_2$, $|B'C'| = d_3$, $|AA'| = L$, $|CC'| = S_1$, $|DD'| = S_2$.

a single speckle into two virtual images. Therefore, for the liquid interface with small depth and deformation to be measured, the virtual image displacement is also small. In this case a larger air gap can be used to increase the virtual image displacement to make the displacement measurement more accurate. On the contrary, when the liquid depth is large and the deformation is large, a smaller airgap should be used to avoid the decorrelation of speckle virtual image.

(2) The speckle patterned glass is immersed in the liquid. In this case, $d_2 = d_3 = 0$, and Eq. (6) is simplified as:

$$h = \frac{S_1}{\tan\gamma} \tag{7}$$

(3) The speckle patterned glass is next to the lower surface of the liquid tank, which means that $d_3 = 0$. Therefore Eq. (6) is simplified as:

$$h = \frac{S_1 - d_2 \tan\alpha_2}{\tan\gamma} \tag{8}$$

Equations (6~8) show that the 2D measurement of the virtual displacements $S_1$ and $S_2$ can achieve the 3D reconstruction of the topography of the liquid interface $h$.

### 2.2. Measurement of virtual displacements

As described in the above subsection, during the measurement of liquid interface, the CCD camera on the top of the liquid interface captures the image of bilayer color speckle patterns. The captured image is coupled by blue and red speckles, which contains virtual displacements $S_1$ and $S_2$, respectively, as shown in Figs. 2(a~c). It needs to be decoupled before the calculation of virtual displacements.

As shown in Fig. 2(c), any pixel position in the speckle pattern has a corresponding RGB value. When decoupling red and blue pixels, follow the principles: (1) When the R value of a certain location is close to the G value and the B value is much greater than the R value, it indicates that there is a blue point at the location; (2) When the B value of a certain location is close to the G value, and the R value is much greater than the B value, a red point appears at that position; (3) When the above two situation are not true, it is a white point. The specific operation is to create two blank images of equal size, and mark them as ImageB and ImageR. And estimate any pixel position $(x, y)$ by:

$$\begin{cases} |B(x,y) - R(x,y)| > D_1 \\ |G(x,y) - R(x,y)| \le D_1 \end{cases} \tag{9}$$

where $D_1$ is set according to the RGB field in Fig. 2(c).

And similarly:

$$\begin{cases} |B(x,y) - R(x,y)| > D_2 \\ |G(x,y) - B(x,y)| \le D_2 \end{cases} \tag{10}$$

where $D_2$ is set according to the RGB field in Fig. 2(c).

When Inequation (9) is true, copy the RGB value at position $(x, y)$ in Fig. 2(c) to position $(x, y)$ of the ImageB. When Inequation (10) holds, copy the RGB value at position $(x, y)$ in Fig. 2(c) to the position $(x, y)$ of ImageR, and fill the rest with white. Finally, the initial blue speckle pattern and the initial red speckle pattern are obtained, which are served as reference patterns for the calculation of $S_1$ and $S_2$.

For the color speckle patterns of deformed liquid interface, the blue and red speckles may overlap when the gap between them is small and the virtual image displacement difference is relatively large. The overlapping area belongs to both the blue and red speckle patterns, so it will be decoupled into the two color speckle patterns at the same time. After that, the color speckle patterns is converted into grayscale for subsequent DIC calculation with reference patterns, respectively. After performing the same processing on all the captured images, the deformed blue and red speckle patterns can be also obtained, as shown in Figs. 2(d~f). All the decoupled color speckle patterns are converted into gray or binarized images using MATLAB. And then, DIC [37–43] is applied to calculate $S_1$ and $S_2$ by the reference and deformed patterns. Finally, the topography of the liquid interface can be reconstructed by combining Equations (6~8).

### 2.3. Reconstruction near crests and troughs

At the crest and trough and their adjacent areas of the liquid interface, the slopes are close to 0. Through light path analysis the virtual displacements of color speckle patterns trends to 0, i.e., $S_1 \approx S_2 \approx 0$. As a result, the denominator of the fraction on the right side of Equations (6~8) trends to 0, resulting a mathematical singularity. In this case, we adopt the following schemes for measuring the topography of the liquid interface $h$ near crest and trough.

As shown in Fig. 1(b), the Snell's law gives:

$$n_1 \sin\alpha_1 = n_3 \sin\beta_1 \tag{11}$$

where $\alpha_1$, $\beta_1$ are the incident and refraction angles at the liquid interface, respectively.

And the geometrical relation at point N gives:

$$\begin{cases} \frac{\partial h}{\partial x} = \tan\beta_1 \\ \beta_1 = \alpha_1 + \gamma \end{cases} \tag{12}$$

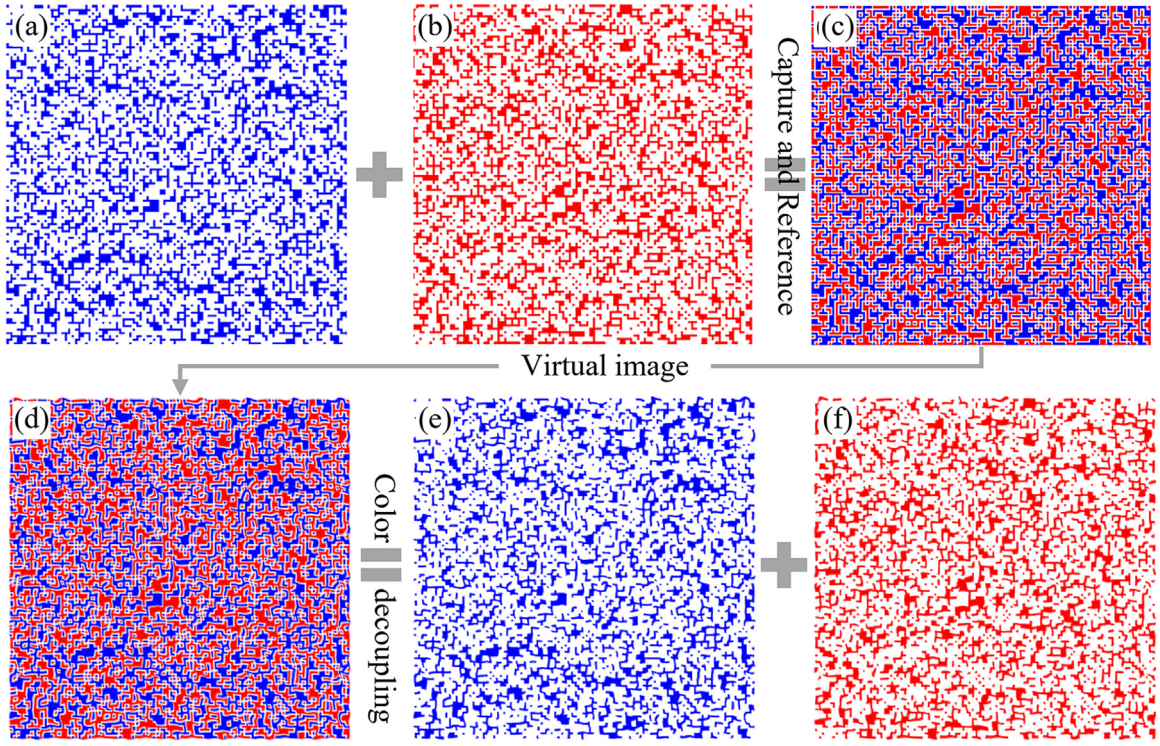


**Fig. 2.** Measurement of virtual displacements $S_1$ and $S_2$ using color speckle patterns. (a, b) Blue and red speckle patterns for measuring $S_1$ and $S_2$, respectively. (c, d) Coupled color speckle pattens when viewed from the top of the interface; (c) is the reference pattern of an initial interface; (d) is the deformed pattern of a deformed interface. (e, f) The decoupled color speckle patterns, serving as the deformed pattern for the displacement measurements. (For interpretation of the references to color in this figure legend, the reader is referred to the web version of this article.).

where the slope of the liquid interface $\frac{\partial h}{\partial x}$ can be determined by combining Eqs. (1, 3, 11, 12), and can be simplified under the first-order Taylor expansion:

$$\frac{\partial h}{\partial x} = \frac{(S_2 - S_1)n_2}{(n_1 - n_3)d_1} \tag{13}$$

It can be seen that the topography reconstruction near crests and troughs can be obtained by integrating Eq. (13):

$$h = \int_{\Omega} \frac{(S_2 - S_1)n_2}{(n_1 - n_3)d_1} \mathrm{d}x \tag{14}$$

where Ω is the crest and trough and their adjacent areas, and is defined by:

$$\Omega \geq \frac{S_2 - S_1}{d_1} \tag{15}$$

In actual calculation, we first measure and calculate $S_1$ and $S_2$ using DIC, and then select an appropriate threshold Ω by Eq. (15) according to the measurement accuracy of displacements.

### 2.4. Sensitivity analysis

The sensitivity determines how small the topography, or the slope of the liquid interface can be measured by the BC-DIC. It can be seen from Eq. (13) that the sensitivity of the liquid interface slope is directly related to the sensitivity of the virtual displacement, which yields by:

$$r_h = \frac{n_2}{(n_1 - n_3)d_1} r_s \tag{16}$$

where $r_s$ is the sensitivity of the virtual displacement measured by DIC (normally 0.1 pixel).

## 3. Experimental

### 3.1. Fabrication of color speckle patterned glass

In the practice of BC-DIC, it is necessary to fabricate a bilayer color speckle glass, of which the most critical step is to design blue and red speckle pattens and print them on very thin films. The blue and red speckle patterns were designed as follows: (1) Generate a random black-white speckle pattern of 1000 × 1000 pixel$^2$ using MATLAB; (2) Record positions of black and white speckles, respectively; (3) Turn black speckles into blue, and white into red, as shown in Fig. 3(a); (4) For the location where red and blue speckles are connected, change it and its neighborhood to white. In this way a blue-red-white speckle pattern is obtained, as shown in Fig. 3(b); (5) The blue and red speckles are extracted separately from the blue-red-white speckle pattern. Thus we obtain the blue-transparent and red-transparent speckle patterns (Figs. 3(c, d)). Finally, the two-color speckle pattens were printed on two transparent PET films, and then were tightly attached to the flat transparent glass (2 mm in thickness) using an ordinary adhesive tape, which the blue speckle film was on the upper surface and the red on the bottom, as shown in Figs. 3(e, f). The thickness of the PET films and their distance to the glass surface is very small compared with that of flat glass and is negligible.

### 3.2. Experimental setup

Fig. 4 shows the experimental setup for the measurement of the topography of a liquid interface using BC-DIC, which was arranged as follows: the fabricated color speckle glass was placed on the hollow support frame with an LED panel (300 × 300 mm$^2$, 24 W) underneath. The blue speckle pattern was upon the red one in the experiments. A color CCD camera (Fastec, IL5–3E2, medium speed) assembled with a lens (Nikon,

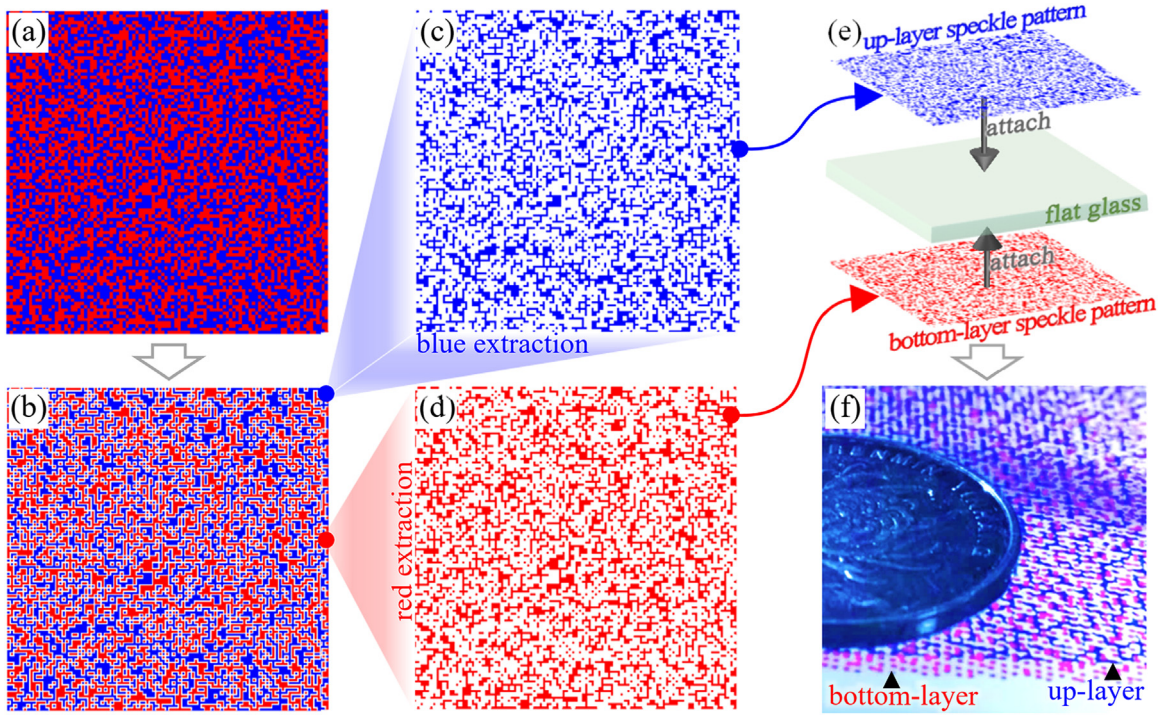


**Fig. 3.** Procession of fabricating bilayer-color speckle patterns. (a) 1000 × 1000 pixel$^2$ color speckle patterns. (b) Generating white gaps. (c) The blue speckle patterns and (d) red speckle patterns. (e) Blue speckle PET film and red speckle PET film tightly attached to the glass. (f) Image from a phone camera. (For interpretation of the references to color in this figure legend, the reader is referred to the web version of this article.).

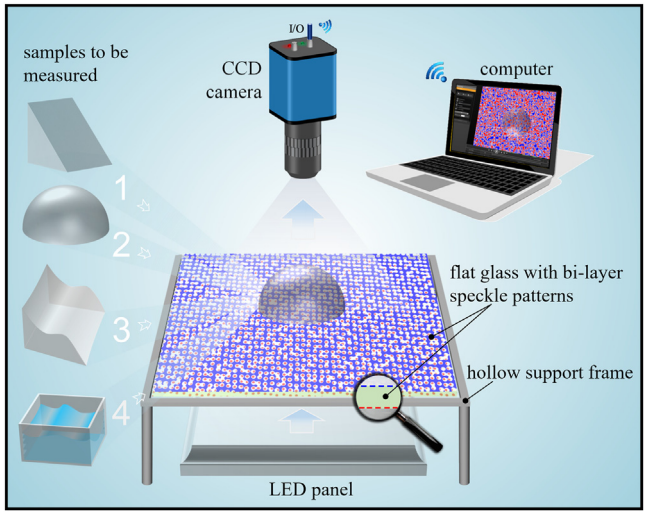


**Fig. 4.** Experimental setup of BC-DIC for the measurement of topography of transparent objects: 1, triangular prism (TP); 2, planoconvex lens (PL); 3, complex transparent surface (CTS); 4, sloshing water surface (SWS).

AF 50mmf/1.8D) was installed directly above the frame. It was adjusted to focus on the bilayer color speckle patterns.

In this paper, we designed four validation experiments to test the feasibility and performance of BC-DIC, i.e., measuring the topographies of the triangular prism (TP), planoconvex lens (PL), complex transparent surface (CTS), and the sloshing water surface (SWS), respectively, as shown in the left of Fig. 4. The parameters for the experiment and the reconstruction are listed in Table 1. The procedures for the experiments were:

**Table 1**
The parameters for the experiment and reconstruction.

| $d_1$ | $d_2$ | $d_3$ | $n_1$ | | | | $n_2$ | $n_3$ |
|---|---|---|---|---|---|---|---|---|
| | | | TP | PL | CTS | SWS | | |
| 2 mm | 5 mm | 0 | 1.516 | 1.516 | 1.520 | 1.333 | 1.520 | 1 |

(1) Adjust the lens to observe the speckle patterns clear and collect a reference image;
(2) Put the test object on the color speckle pattern where under the lens;
(3) Collect the virtual image(s) of the test object. The frame rate was set as 500 fps when measuring the sloshing water surface. The sloshing was achieved by blowing the water surface with a balloon.

## 4. Results and discussion

### 4.1. Decoupling of color speckle patterns

The captured color speckle patterns of the test objects are shown in the left column of Fig. 5. It can be seen that the patterns are coupled with white, blue, red, and blue-red overlap speckles. The overlapping speckles were formed by the incoordination distortion of the bilayer color speckles, which belongs to both the blue and red speckle patterns. The reference and captured color speckle patterns were decoupled by the method presented in §2.2, as shown in the middle and right columns of Fig. 5. After that, the rgb2gray function of MATLAB was used to obtain the corresponding speckle patterns of grayscale. The region of interest (ROI) was selected for the following DIC calculations, as shown in Fig. 5. Considering that the change curvature of the measured objects is not large, so the size of the subset was 41 × 41 pixel$^2$, and the measurement step was set to 1 pixel. In another case for a more distorted geometry/interface of the measured objects, the change of curvature may change greatly, which means that the spatial change rate of displacement is large. Theoretically, finer speckles can better describe this

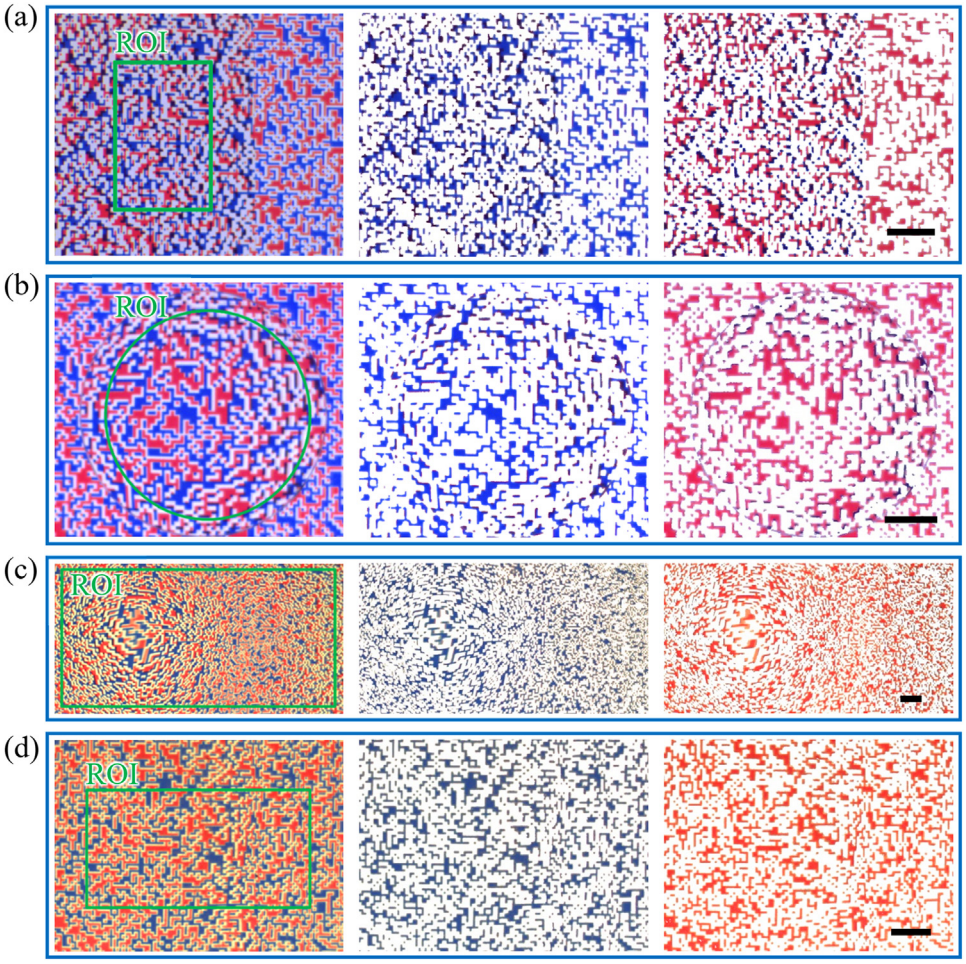


**Fig. 5.** Captured and decoupled speckle patterns of the (a) triangular prism; (b) planoconvex lens; (c) complex transparent surface; (d) sloshing water surface (at a certain moment). Scale bar: 5 mm. (For interpretation of the references to color in this figure legend, the reader is referred to the web version of this article.).

change rate. When there are many overlapping areas in the color speckle pattern, the color of the overlapping area will be close to "black". It is because the blue speckles will filter most of other colors, and so does the red speckles. In this case, the "black" speckles are separated fist with a certain threshold, and then combine them with the decoupled blue or red speckles respectively to achieve the decoupled color speckle patterns. Then, the combined patterns are processed into grayscale or turned into binarization for the subsequent DIC calculation.

### 4.2. Virtual displacement fields

Fig. 6 shows the calculated virtual displacement fields of the test objects using DIC. The first and third columns are $S_1$ and $S_2$, respectively. The second and fourth columns are their coefficient of alienament. The smaller the coefficient of alienament, the more relevant the reference pattern and the deformed pattern. As shown in Fig. 6, all the coefficient of alienament are very small, indicating that the calculated virtual displacement fields are highly reliable for the 3D reconstruction of the test objects.

### 4.3. 3D reconstruction of topography

As we obtained the virtual displacement fields $S_1$ and $S_2$, the topographies of the test objects can be reconstructed according to Equations (6~8). More specifically, the topographies of triangular prism, planoconvex lens and complex transparent surface were reconstructed by Eq. (7). It should be noted that the reconstruction near crests and troughs was achieved by the scheme introduced in §2.3. Fig. 7 shows the reconstructed topographies of the test objects. It can be seen that all the topographies are very smooth and conform to the actual ones in appearance.

The topographies of the sloshing water surface at different moments were reconstrued by Eq. (8) due to the presence of the bottom glass of the water tank between the color speckle patterns and the liquid. Similarly, the reconstruction of the liquid interface near crests and troughs was achieved by the scheme introduced in §2.3. Fig. 8 is the reconstructed topographies of the water surface at different moments, which shows the process of a swaying water wave propagating and attenuating from front to back.

### 4.4. Error estimation

After the topography of the test objects were measured using BC-DIC, it was compared with the real topography of the objects to estimate the measurement error of the method. In this paper, we calculated the measurement error of the triangular prism and planoconvex lens, as shown in Fig. 9. It can be seen in Figs. 9(a, d) that the measured heights are consistent with the corresponding real height. Figs. 9(b, e) were plotted by taking some cross-sections for observation, which also show that the measured values almost all fall on the curves of the real heights. We also calculated the error fields in Figs. 9(c, f), showing that the relative error is within 2.09% for the measurement of triangular prism and 4.79% for the planoconvex lens. This indicates that the developed BC-DIC is feasible for the measurement of the topography of transparent objects, as well as the topography of the liquid interface. It should be noted that when measuring objects with small virtual image displacement, it is necessary to process the image with special precautions, such as Forsey and

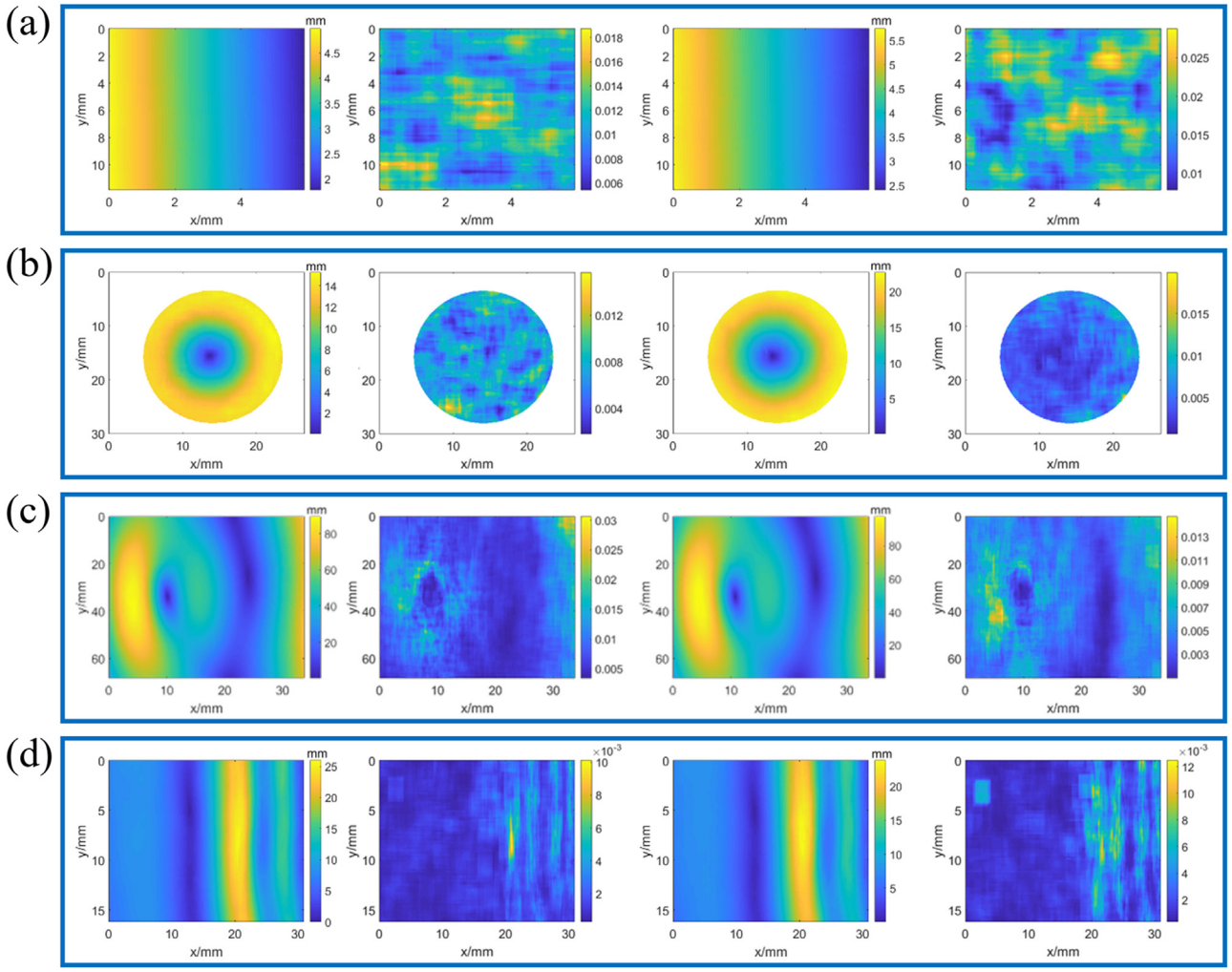


**Fig. 6.** Calculated displacement fields $S_1$ and $S_2$, corresponding to the first and third columns, respectively. And their coefficient of alienament (the second and fourth columns) of reference patterns and deformed patterns using DIC. (a) Triangular prism; (b) planoconvex lens; (c) complex transparent surface; (d) sloshing water surface.

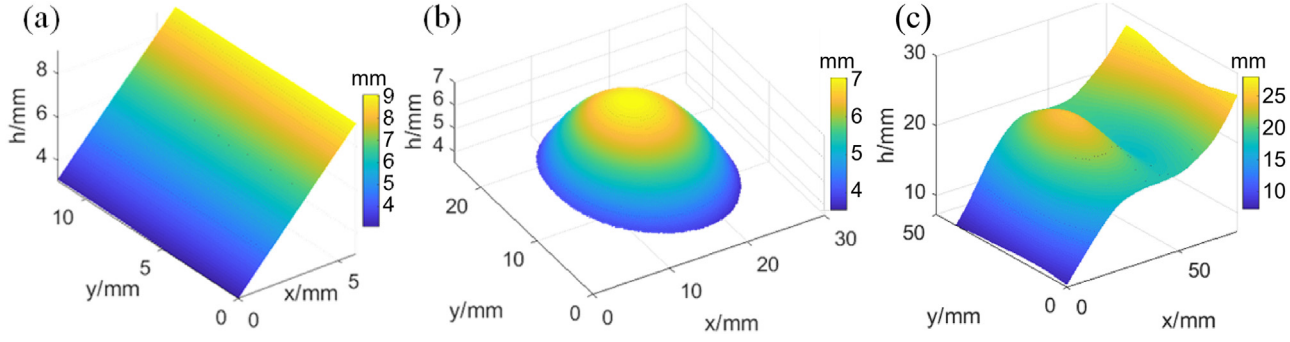


**Fig. 7.** The reconstructed topography of the (a) triangular prism; (b) planoconvex lens and (c) complex transparent surface.

Gungor [44], and Baldi [45] did in their studies, which can improve the measurement accuracy further.

## 5. Conclusions

We report a simple but effective BC-DIC method for the measurement of the topography of the liquid interface. The principle and the theory of the method, that is, how to reconstruct the topography by correlating the interface height and the virtual distortion of the beneath bilayer color speckle patterns, were detailed discussed and deduced. Validation experiments were carried out to measure the topographies of the triangular prism, planoconvex, complex transparent surface, and sloshing water surface. The results showed that BC-DIC is feasible and the accuracy is good for measuring the topography of the transparent objects, including the liquid interface. The advantages of the developed methods include: very simple instrument and operation; convenient calculation with no need for iteration and initial values; high reconstruction efficiency; feasible to measure topography with large slope and amplitude. The limit of topography detection in the current study is that since the spacing between the bilayer speckle patterns cannot be too small (other-

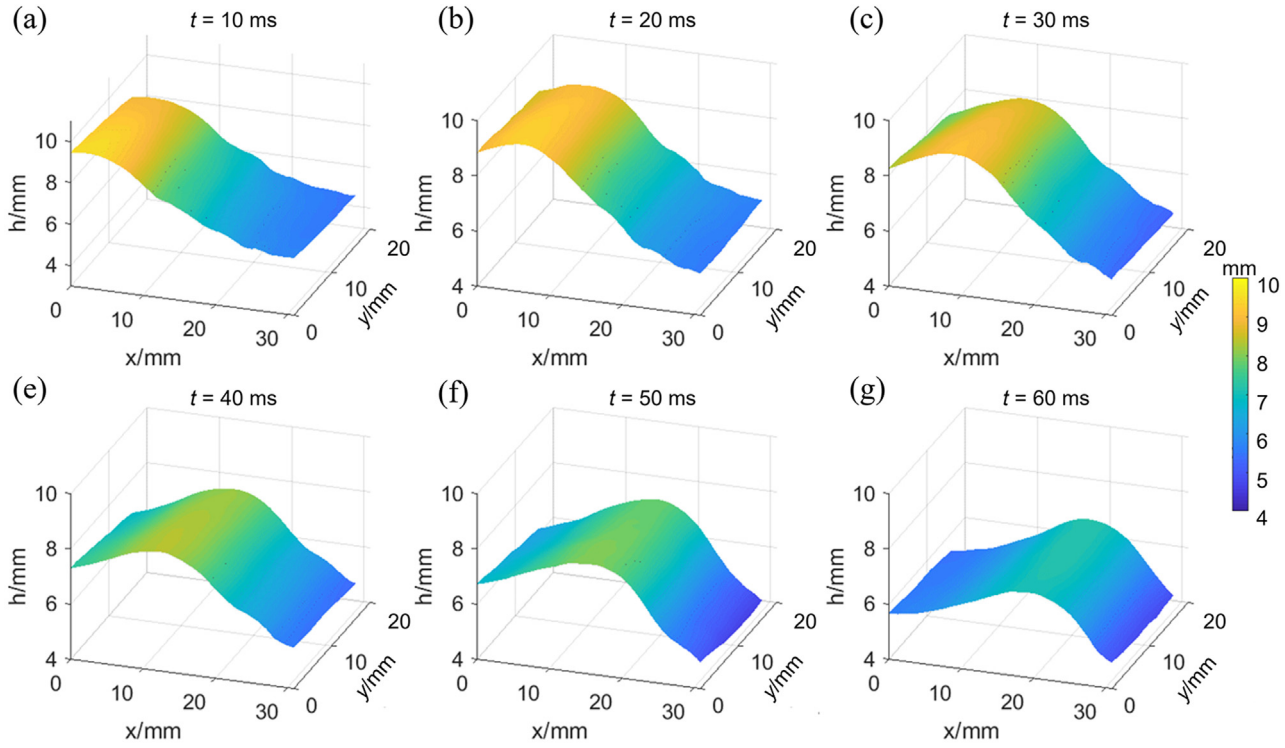


**Fig. 8.** The reconstructed topographies of the sloshing water surface at different moments.

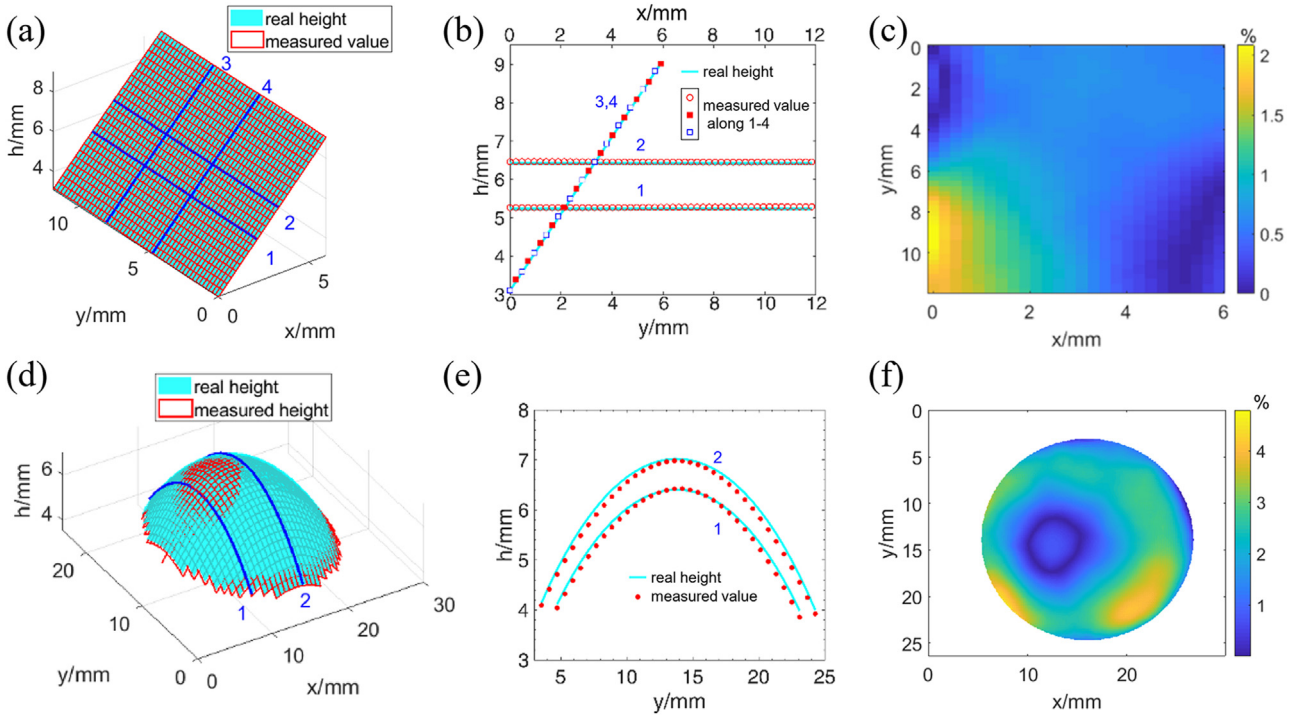


**Fig. 9.** Comparison of the measurement value and the real height. (a) The measured and the real topography of the triangular prism; (b) cross-sections in (a); (c) the relative error field of the triangular prism shape measurement. (d) The measured and the real topography of the planoconvex lens; (e) cross-sections in (d); (f) the relative error field of the planoconvex lens shape measurement. (For interpretation of the references to color in this figure legend, the reader is referred to the web version of this article.).

wise the difference between $S_1$ and $S_2$ is too small to make the measurement inaccurate), it is necessary to use a lens with a large depth of field. As practical implications of BC-DIC, it helps to study surface and interface phenomena, such as fuel sloshing, hydrodynamics of water-walking insects, and surface tension etc.

## Declaration of Competing Interest

The authors declare that they have no known competing financial interests or personal relationships that could have appeared to influence the work reported in this paper.

## CRediT authorship contribution statement

**Yao Huang:** Investigation, Visualization, Validation, Writing – original draft. **Xianfu Huang:** Supervision, Conceptualization, Formal analysis, Writing – original draft, Writing – review & editing, Resources, Funding acquisition. **Menglin Zhong:** Formal analysis. **Zhanwei Liu:** Supervision, Methodology, Writing – review & editing, Resources, Funding acquisition.

## Acknowledgements

This work was jointly supported by the National Natural Science Foundation of China (NSFC), Grant No. 11972084, 12032019, the Youth Innovation Promotion Association Chinese Academy of Sciences (CAS), and the CAS Key Research Program of Frontier Sciences (Grant No. QYZDJ-SSW-JSC019).

## References

[1] Ibrahim RA, Pilipchuk VN, Ikeda T. Recent advances in liquid sloshing dynamics. Appl Mech Rev 2001;54(2):133–99.
[2] Yang Y, Liu Z-W, Shi W-X, Huang X-F. Accurate measurement of nonlinear liquid sloshing. AIAA J 2015;53(3):771–9.
[3] Liu D, Lin P. A numerical study of three-dimensional liquid sloshing in tanks. J Comput Phys 2008;227(8):3921–39.
[4] Rafiee A, Pistani F, Thiagarajan K. Study of liquid sloshing: numerical and experimental approach. Comput Mech 2011;47(1):65–75.
[5] Hu DL, Chan B, Bush JWM. The hydrodynamics of water strider locomotion. Nature 2003;424(6949):663–6.
[6] Liu S, Liu Z-W, Shi W-X. A source for the excellent floating ability of a water strider. Chinese Phys Lett 2014;31(10):106801.
[7] Koh J-S, Yang E, Jung G-P, Jung S-P, Son Jae H, Lee S-I, Jablonski Piotr G, Wood Robert J, Kim H-Y, Cho K-J. Jumping on water: surface tension–dominated jumping of water striders and robotic insects. Science 2015;349(6247):517–21.
[8] Hu DL, Bush JWM. The hydrodynamics of water-walking arthropods. J Fluid Mech 2010;644:5–33.
[9] Bush JWM, Hu DL, Prakash M. The integument of water-walking arthropods: form and function. Adv Insect Physiol 2007;34:117–92.
[10] Zhao Y-P. Physical mechanics of surfaces and interfaces. Beijing: Science Press; 2012.
[11] Pregent S, Adams S, Butler MF, Waigh TA. The impact and deformation of a viscoelastic drop at the air–liquid interface. J Colloid Interf Sci 2009;331(1):163–73.
[12] Hoffman RL. A study of the advancing interface. I. Interface shape in liquid—Gas systems. J Colloid Interf Sci 1975;50(2):228–41.
[13] Ma X, Zhong M, He Y, Liu Z, Li Z. Fingering instability in marangoni spreading on a deep layer of polymer solution. Phys Fluids 2020;32(11):112112.
[14] Yuan Q, Zhao Y-P. Multiscale dynamic wetting of a droplet on a lyophilic pillar-arrayed surface. J Fluid Mech 2013;716:171–88.
[15] Yu Y-S, Wang Z, Zhao Y-P. Experimental and theoretical investigations of evaporation of sessile water droplet on hydrophobic surfaces. J Colloid Interf Sci 2012;365(1):254–9.
[16] Gennes P-G, Brochard-Wyart F, Quéré D, Reisinger A, Widom B. Capillarity and wetting phenomena: drops, bubbles, pearls, waves. Springer; 2004.
[17] Thorsten B, Wansong L, Christoph von K, Werner POJ. High-resolution 3d shape measurement on specular surfaces by fringe reflection. ProcSPIE 2004.
[18] Huang L, Ng CS, Asundi AK. Dynamic three-dimensional sensing for specular surface with monoscopic fringe reflectometry. Opt Express 2011;19(13):12809–14.
[19] Cobelli PJ, Maurel A, Pagneux V, Petitjeans P. Global measurement of water waves by fourier transform profilometry. Expe Fluids 2009;46(6):1037.
[20] Vinnichenko NA, Pushtaev AV, Plaksina YY, Uvarov AV. Measurements of liquid surface relief with moon-glade background oriented schlieren technique. Exp Therm Fluid Sci 2020;114:110051.
[21] Liu Z, Guo J, Shi W, Huang X, Xie H. Transmission-speckle correlation for measuring dynamic deformation of liquid surface. Opt Laser Eng 2015;65:110–16.
[22] Liu Z, Huang X, Xie H. A novel orthogonal transmission-virtual grating method and its applications in measuring micro 3-D shape of deformed liquid surface. Opt Laser Eng 2013;51(2):167–71.
[23] Huang X, Dong H, Liu Z, Zhao Y-P. Probing micro-newton forces on solid/liquid/gas interfaces using transmission phase shift. Langmuir 2019;35(16):5442–7.
[24] Zhong M, Huang X, Dong H, Liu Z. 3d shape measurement of complex transparent liquid surfaces using monoscopic deformed fringe transmissometry. Meas Sci Technol 2019;30(11):115201.
[25] Shi W, Huang X, Liu Z. Transmission-lattice based geometric phase analysis for evaluating the dynamic deformation of a liquid surface. Opt Express 2014;22(9):10559–69.
[26] Fouras A, Hourigan K, Kawahashi M, Hirahara H. An improved, free surface, topographic technique. J Visual 2006;9:49–56.
[27] Moisy F, Rabaud M, Salsac K. A synthetic schlieren method for the measurement of the topography of a liquid interface. Expe Fluids 2009;46(6):1021.
[28] Moisy F, Michon G-J, Rabaud M, Sultan E. Cross-waves induced by the vertical oscillation of a fully immersed vertical plate. Phys Fluids 2012;24(2):022110.
[29] Moisy F, Rabaud M, Pinsolle E. Measurement by digital image correlation of the topography of a liquid interface. In: ISFV13 - 13th International Symposium on Flow Visualization FLUVISU12 - 12th French Congress on Visualization in Fluid Mechanics. France: Nice; 2008.
[30] Fouras A, Lo Jacono D, Sheard GJ, Hourigan K. Measurement of instantaneous velocity and surface topography in the wake of a cylinder at low reynolds number. J Fluids Struct 2008;24(8):1271–7.
[31] Tang H, Dong H, Liu Z. Study on dynamic deformation synchronized measurement technology of double-layer liquid surfaces. Opt Laser Eng 2017;98:205–16.
[32] Kolaas J, Riise BH, Sveen K, Jensen A. Bichromatic synthetic schlieren applied to surface wave measurements. Expe Fluids 2018;59(8):128.
[33] Gomit G, Chatellier L, Calluaud D, David L. Free surface measurement by stereo-refraction. Expe Fluids 2013;54(6):1540.
[34] Chatellier L, Jarny S, Gibouin F, David L. A parametric piv/dic method for the measurement of free surface flows. Expe Fluids 2013;54(3):1488.
[35] Chien C-H, Su T-H, Huang C-J, Chao Y-J, Yeh W-L, Lam P-S. Application of digital image correlation (DIC) to sloshing liquids. Opt Laser Eng 2019;115:42–52.
[36] Yu L, Pan B. Full-frame, high-speed 3d shape and deformation measurements using stereo-digital image correlation and a single color high-speed camera. Opt Laser Eng 2017;95:17–25.
[37] Jiang L, Xie H, Pan B. Speeding up digital image correlation computation using the integral image technique. Opt Laser Eng 2015;65:117–22.
[38] Pan B, Qian K, Xie H, Asundi A. Two-dimensional digital image correlation for in-plane displacement and strain measurement: a review. Meas Sci Technol 2009;20(6):062001.
[39] Pan B, Xie H, Wang Z, Qian K, Wang Z. Study on subset size selection in digital image correlation for speckle patterns. Opt Express 2008;16(10):7037–48.
[40] Wang Z, Kieu H, Nguyen H, Le M. Digital image correlation in experimental mechanics and image registration in computer vision: similarities, differences and complements. Opt Laser Eng 2015;65:18–27.
[41] Hua T, Xie H, Pan B, Wang Q, Dai F. A new mark shearing technique for strain measurement using digital image correlation method. Rev Sci Instrum 2008;79(10):105101.
[42] Nguyen H, Liang J, Wang Y, Wang Z. Accuracy assessment of fringe projection profilometry and digital image correlation techniques for three-dimensional shape measurements. J Phys-Photonics 2021;3(1):014004.
[43] Gao J, Shang H. Deformation-pattern-based digital image correlation method and its application to residual stress measurement. Appl Opt 2009;48(7):1371–81.
[44] Forsey A, Gungor S. Demosaicing images from colour cameras for digital image correlation. Opt Laser Eng 2016;86:20–8.
[45] Baldi A. Digital image correlation and color cameras. Exp Mech 2018;58(2):315–33.